Computational Materials Science 48 (2010) 258–266

Contents lists available at ScienceDirect

Computational Materials Science

journal homepage: www.elsevier.com/locate/commatsci

Effect of strain and oxygen vacancies on the structure of 180° ferroelectric domain walls in $PbTiO_3$

Arzhang Angoshtari, Arash Yavari *

School of Civil and Environmental Engineering, Georgia Institute of Technology, Atlanta, GA 30332, United States

ARTICLE INFO

Article history:
Received 5 November 2009
Received in revised form 4 January 2010
Accepted 8 January 2010
Available online 2 February 2010

Keywords:
Ferroelectrics
Domain walls
Lattice statics
Oxygen vacancies

ABSTRACT

In this paper, we study the effect of normal and shear strains and oxygen vacancies on the structure of 180° ferroelectric domain walls in $PbTiO_3$. It is known that oxygen vacancies move to the domain walls and pin them. Hence, we assume a periodic arrangement of oxygen vacancies on both Pb-centered and Ti-centered domain walls in $PbTiO_3$. We use a semi-analytic anharmonic lattice statics method for obtaining the relaxed configurations using a shell potential. In agreement with recent ab initio calculations, we observe that a Pb-centered domain wall with oxygen vacancies is not stable even under strain. Our semi-analytic calculations for $PbTiO_3$ show that oxygen vacancies affect the structure of 180° domain walls significantly but do not have a considerable effect on the thickness of domain walls; they broaden the domain walls by about 50%. We also study the effect of normal and shear strains on both perfect and defective 180° domain walls. We observe that normal and shear strains affect the structure but do not change the domain wall thickness.

1. Introduction

Ferroelectric perovskites have been the focus of intense research in recent years because of their potential applications in high strain actuators, high density storage devices, etc. [2]. It is known that macroscopic properties of ferroelectrics are strongly dependent on domain walls, which are extended two-dimensional defects. Any fundamental understanding of ferroelectricity in perovskites requires a detailed understanding of domain walls in the nanoscale as these defects are atomically sharp (see [8] and references therein). Theoretical studies of domain walls have revealed many of their interesting features. From both ab inito calculations [16,18,20,21] and anaharmonic lattice statics calculations [32] it is now known that ferroelectric domain walls are atomically sharp. In all these studies, the structure calculations have been done for perfect domain walls and free of strain. However, domain walls interact with other types of defects and mainly with oxygen vacancies and this may affect the structure and properties of domain walls. Strain may also have a significant effect on domain wall structure.

It is known that the presence of point defects can have important effects on the properties of perovskites. For example, Bujakiewicz-Koronska and Natanzon [4] show that point defects alter the elastic constants of $Na_{1/2}Bi_{1/2}TiO_3$ significantly. In this paper, we study the effect of oxygen vacancies and normal and shear strains on the structure of 180° ferroelectric domain walls. It is known that oxygen vacancies move to the domain walls and pin them and thus we assume a periodic arrangement of oxygen vacancies on both Pb-centered and Ti-centered domain walls. We use a semi-analytic anharmonic lattice statics method for obtaining the relaxed configurations using a shell potential. In agreement with the recent ab initio calculations, we observe that a Pb-centered domain wall with oxygen vacancies is not stable even under strain. Our semi-analytic solutions for $PbTiO_3$ show that oxygen vacancies increase the thickness of the domain wall by about 50%. This is different from the results of a recent experimental measurements of 90° domain walls in $PbTiO_3$ using AFM by Shilo et al. [28]. They observed that there is a large variation in domain wall thickness with respect to position (0.5–4.0 nm). This is not very surprising as vacancies may interact differently with different types of domain walls. In our calculations, we observe that oxygen vacancies have a significant effect on the detailed structure of 180° domain walls. Our result is in agreement with a recent continuum study of interaction of oxygen vacancies with domain walls [30]. Xiao et al.'s continuum model predicts that 180° and 90° domain walls have quite different interactions with oxygen vacancies.

There are several works in the literature on the effect of strain on ferroelectric domain walls showing that strain can have important effects on domain walls. For example, both experiments [27] and ab initio calculations [29] show that shear stress applied to 90° domain walls in $PbTiO_3$ develops polarization reorientation through a domain wall movement perpendicular to itself known as stress-induced domain switching. To our best knowledge, there

* Corresponding author. Tel.: +1 404 894 2436; fax: +1 404 894 2278.
E-mail address: arash.yavari@ce.gatech.edu (A. Yavari).

0927-0256/$ - see front matter © 2010 Elsevier B.V. All rights reserved.
doi:10.1016/j.commatsci.2010.01.006

are no atomistic calculations in the literature on the effect of strain on the structure of 180° domain walls in $PbTiO_3$.

This paper is structured as follows: In Section 2 we briefly review the previous studies of ferroelectric domain walls. We then present the main ideas of anharmonic lattice statics analysis of perfect and defective ferroelectric domain walls under strain. In Section 3 we report some numerical results for 180° domain walls in $PbTiO_3$ using a shell potential. Conclusions are given in Section 4.

2. Ferroelectric domain walls

Ferroelectric domain walls have been studied extensively both theoretically and experimentally. For recent experimental investigations see [28,9] and references therein. Shilo et al. [28] studied the structure of 90° domain walls in $PbTiO_3$ using atomic force microscopy (AFM). They measured the surface topography of a given sample and compared it with a displacement field that is obtained from the Devonshire–Ginzburg–Landau phenomenological model. They calculated the thickness of two domain walls at two different positions and observed thicknesses of 0.5 nm and 4.0 nm for the two domain walls. They then conjectured that presence of point defects is responsible for this variation. Lee et al. [14] used a two-dimensional square lattice model that has a continuum order parameter interacting with a lattice of Ising spins, where the Ising spins model the presence or absence of point defects. They show that depending on the parameters used in their model, one can reproduce the main features of the experimentally observed variation in domain wall thickness in Shilo et al.'s [28] experiments. However, one should note that Shilo et al.'s results may not apply to all types of domain walls as they studied only the 90° domain walls.

Ab initio calculations of He and Vanderbilt [11] show that oxygen vacancies have a tendency to move to domain walls and pin them. They also observed that defective domain walls are Ti-centered. In their calculations, they had to assume a periodic array of domain walls with a high density of charge-neutral oxygen vacancies. There have also been other ab initio calculations of point defects in $PbTiO_3$ in the bulk [18,19,6]. Xiao et al. [30] studied the effect of oxygen vacancies on the structure of domain walls in tetragonal $BaTiO_3$ using a continuum theory that takes into account the fact that ferroelectrics are wide-band-gap semiconductors. In their numerical calculations they observed that 180° and 90° domain walls behave differently in response to oxygen vacancies. In particular, they saw charge accumulation near 90° domain walls with a potential drop across the wall while these were absent in the case of 180° domain walls.

2.1. Anharmonic lattice statics of domain walls

Method of lattice statics was introduced by Matsubara [15] and Kanazaki [12] and was extensively used by Born and Huang [3]. For more details and history see Ortiz and Phillips [17] and Yavari et al. [31,32]. In this paper, we study the possibility of domain wall broadening by oxygen vacancies in the case of 180° domain walls in $PbTiO_3$. We also study the effect of shear and normal strains on both defect-free domain walls and domain walls with oxygen vacancies.

We present a semi-analytical solution of structure of 180° domain walls using an anharmonic lattice statics method [31,32]. From ab initio calculations of oxygen vacancies in $PbTiO_3$ [11] and also molecular dynamics simulations of $CaTiO_3$ [5], we know that oxygen vacancies have a tendency to move to the domain walls and pin them. Therefore, we study the structure of domain walls with oxygen vacancies sitting on the wall. To be able to solve the discrete governing equations analytically we need to assume some periodicity for the collection of vacancies on the wall. We consider a 180° domain wall in an infinite crystal and assume that oxygen vacancies are periodically arranged on the domain wall. Thus, the only restrictive assumption is the periodicity and high density of vacancies on the domain wall. In reality, oxygen vacancies can be distributed randomly and have a smaller density. However, the results from our calculations can still provide some important quantitative information on the effect of oxygen vacancies on the structure of 180° domain walls in the nanoscale.

2.2. Defect-free 180° domain walls

We use a shell potential for modeling $PbTiO_3$ [1] and all the calculations are performed for $T = 0$ K. Denoting the collection of cores and shells by $\mathscr{L}$, $i \in \mathscr{L}$ represents a core (or shell) in the collection. In a shell potential, total energy has the following form [7,25,26]:

$$\mathscr{E}(\{\mathbf{x}^i\}_{i\in\mathscr{L}}) = \mathscr{E}_{\text{short}}(\{\mathbf{x}^i\}_{i\in\mathscr{L}}) + \mathscr{E}_{\text{long}}(\{\mathbf{x}^i\}_{i\in\mathscr{L}}) + \mathscr{E}_{\text{core-shell}}(\{\mathbf{x}^i\}_{i\in\mathscr{L}}), \tag{2.1}$$

where $\{\mathbf{x}^i\}_{i\in\mathscr{L}}$ is the current position of cores and shells. Short range energy depends explicitly on the position vectors of the massless shells. Long range energy is the Coulombic energy of all cores and shells, excluding core-shell interaction in the same atom. The core-shell energy prevents the shell collapse in each atom and is usually a polynomial function of the pairwise distance of core and shell in a given atom. In the equilibrium configuration $\mathscr{B} = \{\mathbf{x}^i\}_{i\in\mathscr{L}} \subset \mathbb{R}^3$, energy attains a local minimum, i.e.

$$\frac{\partial \mathscr{E}}{\partial \mathbf{x}^i} = \mathbf{0} \quad \forall i \in \mathscr{L}. \tag{2.2}$$

However, in the case of a defective crystal, the problem is that we do not know the relaxed configuration a priori. Thus, we start with a reference configuration $\mathscr{B}_0 = \{\mathbf{x}_0^i\}_{i\in\mathscr{L}}$ that is not necessarily force free [31]. In the case of a 180° domain wall, $\mathscr{B}_0$ is a nominal defect, i.e., a configuration in which cores and shells on the left and right sides of the wall have their positions in the bulk configurations corresponding to P_s and $-P_s$, respectively, where P_s is the spontaneous polarization (see Fig. 2.1). This reference configuration is not force free. Let us denote the discrete field of unbalanced forces by

$$\mathbf{f} = \left\{ -\frac{\partial \mathscr{E}}{\partial \mathbf{x}^i}(\mathscr{B}_0) \right\}_{i\in\mathscr{L}}. \tag{2.3}$$

In anharmonic lattice statics one finds the discrete deformation mapping $\varphi : \mathscr{B}_0 \to \mathscr{B}$ that takes the chosen nominal defect to its relaxed configuration. Note that a different choice of reference configuration $\mathscr{B}_0'$ leads to a different discrete deformation mapping $\varphi' : \mathscr{B}_0' \to \mathscr{B}$. If the two reference configurations are 'close', i.e., they are in the same energy well, we would converge to the same relaxed configuration. The discrete deformation map is found semi-analytically as follows.

Taylor expanding (2.2) about the reference configuration and ignoring terms higher than quadratic in displacements, one obtains the following linearized governing equations:

$$\frac{\partial \mathscr{E}}{\partial \mathbf{x}^i}(\mathscr{B}_0) + \sum_j \frac{\partial^2 \mathscr{E}}{\partial \mathbf{x}^j \partial \mathbf{x}^i}(\mathscr{B}_0)\left(\mathbf{x}^j - \mathbf{x}_0^j\right) = \mathbf{0}, \tag{2.4}$$

or

$$\sum_j \frac{\partial^2 \mathscr{E}}{\partial \mathbf{x}^j \partial \mathbf{x}^i}(\mathscr{B}_0)\mathbf{u}^j = \mathbf{f}_i \quad \forall i \in \mathscr{L}, \tag{2.5}$$

where $\mathbf{u}^j = \mathbf{x}^j - \mathbf{x}_0^j$. For a defect-free domain wall, atoms (cores, shells) of the same type parallel to the wall will have the same displacement vectors. This symmetry simplifies the linear equations

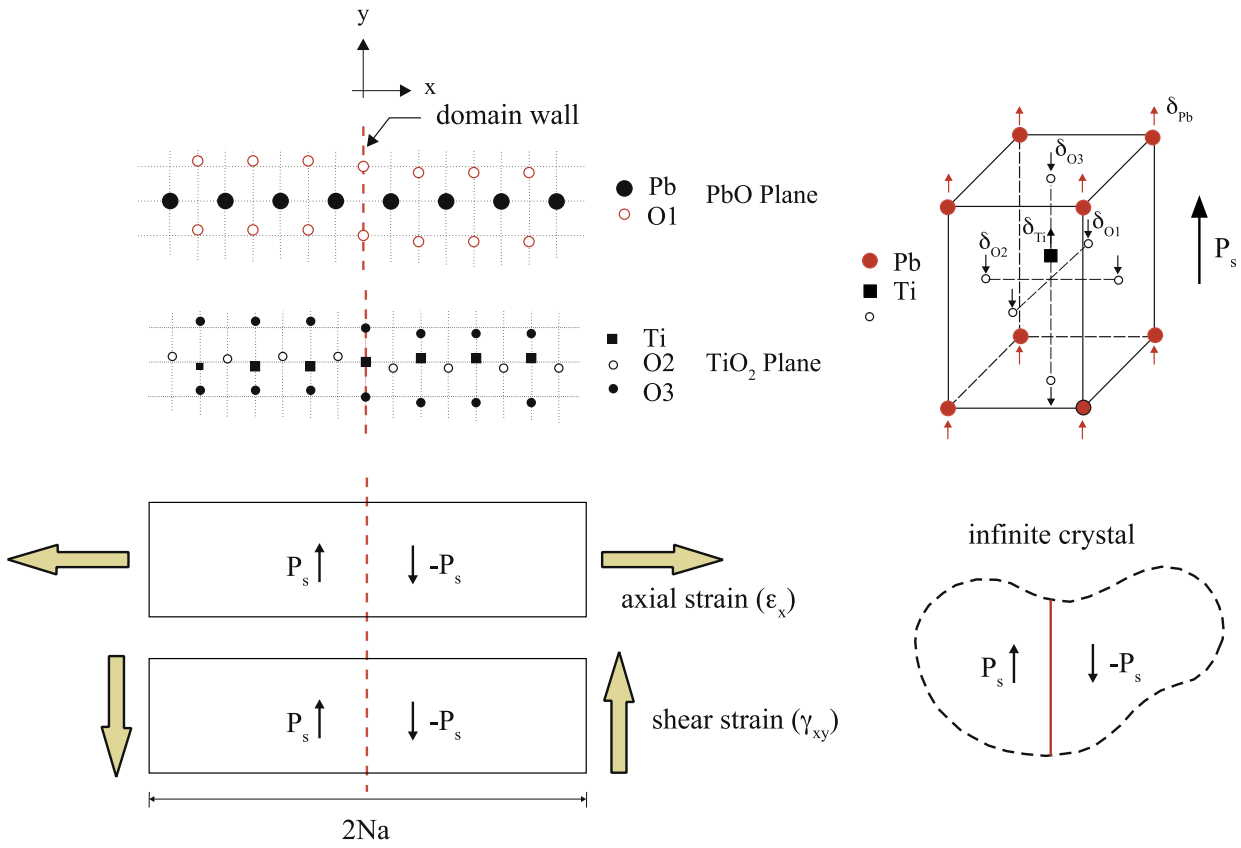

Fig. 2.1. Reference configuration for a Ti-centered 180° domain wall in PbO and TiO_2 planes. Note that cores and shells on the domain wall have no relative shifts and cores and shells on the left and right sides of the wall have opposite relative shifts. a and N are lattice parameter and size of the simulation box, respectively.

(2.4) considerably [13]. Assume that the defective crystal $\mathscr{L}$ has a 1-D symmetry reduction, i.e., it can be partitioned into two-dimensional equivalence classes, i.e.

$$\mathscr{L} = \bigsqcup_{\alpha\in\mathbb{Z}} \bigsqcup_{I=1}^{M} \mathscr{S}_{I\alpha}(i), \tag{2.6}$$

where $\mathscr{S}_{I\alpha}(i)$ is the equivalence class of all the atoms of type I and index α with respect to atom i. Here we assume that $\mathscr{L}$ is a multilattice of M simple lattices (for $PbTiO_3$, $M = 10$). Particle i is an arbitrary core (shell) and assuming that it is in the nth equivalence class of its type, $\mathscr{S}_{I\alpha(i)}$ is the set of those cores (shells) of type I that are in the equivalence class $n + \alpha$. For a free surface, for example, each equivalence class is a set of cores (shells) lying on a plane parallel to the free surface. Using this partitioning one can write

$$\sum_j \frac{\partial^2 \mathscr{E}}{\partial \mathbf{x}^j \partial \mathbf{x}^i}(\mathscr{B}_0)\left(\mathbf{x}^i - \mathbf{x}_0^j\right) = \sum_{\alpha=-\infty}^{\infty} {\sum_{I=1}^{M}}' \sum_{j\in\mathscr{S}_{I\alpha(i)}} \frac{\partial^2 \mathscr{E}}{\partial \mathbf{x}^j \partial \mathbf{x}^i}(\mathscr{B}_0)\left(\mathbf{x}^{I\alpha} - \mathbf{x}_0^{I\alpha}\right), \tag{2.7}$$

where the prime on the second sum means that the term $\alpha = 0$, $I = i$ is omitted. The linearized discrete governing equations are written as

$$\sum_{\alpha=-\infty}^{\infty} {\sum_{I=1}^{M}}' \mathbf{K}_{il\alpha}\mathbf{u}^{I\alpha} + \left[-\sum_{\alpha=-\infty}^{\infty} {\sum_{I=1}^{M}}' \mathbf{K}_{il\alpha}\right]\mathbf{u}^i = \mathbf{f}_i, \tag{2.8}$$

where

$$\mathbf{K}_{il\alpha} = \sum_j \frac{\partial^2 \mathscr{E}}{\partial \mathbf{x}^j \partial \mathbf{x}^i}(\mathscr{B}_0), \quad \mathbf{f}_i = -\frac{\partial \mathscr{E}}{\partial \mathbf{x}^i}(\mathscr{B}_0),$$
$$\mathbf{u}^{I\alpha} = \mathbf{x}^{I\alpha} - \mathbf{x}_0^{I\alpha} = \mathbf{x}^j - \mathbf{x}_0^j \qquad \forall j \in \mathscr{S}_{I\alpha(i)}. \tag{2.9}$$

Unit cell displacement vectors are defined as $\mathbf{X}_n = (\mathbf{u}_n^1, \ldots, \mathbf{u}_n^M)^{\mathrm{T}}$. Now the governing equations in terms of unit cells displacements are

$$\sum_{\alpha=-m}^{m} \mathbf{A}_\alpha(n)\mathbf{X}_{n+\alpha} = \mathbf{F}_n \quad n \in \mathbb{Z}, \tag{2.10}$$

where $\mathbf{A}_\alpha(n) \in \mathbb{R}^{3M\times 3M}$, $\mathbf{X}_n$, $\mathbf{F}_n \in \mathbb{R}^{3M}$ and m is the range of interaction of unit cells and $m = 1$ would be accurate enough for the shell potential [32]. Eq. (2.10) is a linear vector-valued ordinary difference equation of order $2m$ with variable coefficient matrices and the unit cell force vectors and the unit cell stiffness matrices are defined as

$$\mathbf{F}_n = \begin{pmatrix} \mathbf{f}_{1n} \\ \vdots \\ \mathbf{f}_{Mn} \end{pmatrix}, \quad \mathbf{A}_\alpha(n) = \begin{pmatrix} \mathbf{K}_{11\alpha} & \mathbf{K}_{12\alpha} & \cdots & \mathbf{K}_{1M\alpha} \\ \mathbf{K}_{21\alpha} & \mathbf{K}_{22\alpha} & \cdots & \mathbf{K}_{2M\alpha} \\ \vdots & \vdots & \cdots & \vdots \\ \mathbf{K}_{M1\alpha} & \mathbf{K}_{M2\alpha} & \cdots & \mathbf{K}_{MM\alpha} \end{pmatrix} \qquad n \in \mathbb{Z}. \tag{2.11}$$

Note that $\mathbf{A}_\alpha(n)$ explicitly depends on n and this reflects the fact that close to the domain wall force constants may change.

2.3. 180° Domain walls with oxygen vacancies

It is known for quite sometime that for a large enough number of oxygen vacancies in perovskites one would see a self-organized planar arrangement of oxygen vacancies (see [24,10] and references therein. See also Zhang [33] for atomistic calculations and discussions on oxygen vacancies in $BaTiO_3$ and their different possible arrangements). Therefore, similar to the ab initio calculations of He and Vanderbilt [11], we assume that oxygen vacancies

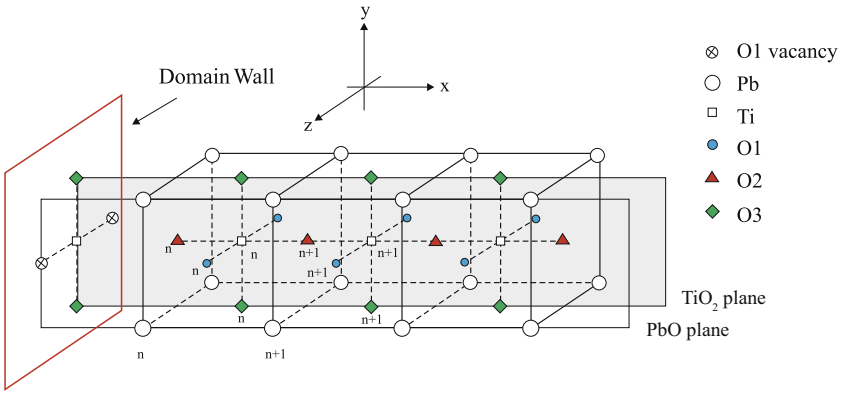

Fig. 2.2. Unit cell indexing in the reference configuration of a Ti-centered 180° domain wall. Note that because of symmetry displacements in the z-direction are all zero.

interact with a domain wall and have a planar structure coinciding with the domain wall.

Eq. (2.10) is the governing equation for a defective domain wall as long as the oxygen vacancies are arranged periodically on the domain wall. However, $\mathbf{A}_\alpha(n)$ and $\mathbf{F}_n$ would change, in general. We can simplify the solution of the discrete boundary-value problem even further by noting that the displacements of cores and shells on the left side of the wall are related to those on the right side of the wall, i.e., the wall is a reflection symmetry plane. This reduces (2.10) to an ordinary difference equation on $\mathbb{N}_2$, i.e.,

$$\mathbf{A}_{-1}\mathbf{X}_{n-1} + \mathbf{A}_0\mathbf{X}_n + \mathbf{A}_1\mathbf{X}_{n+1} = \mathbf{F}_n \quad n \geqslant 2, \tag{2.12}$$

with the following boundary equations:

$$\mathbf{A}_{-1}(0)\mathbf{X}_{-1} + \mathbf{A}_1(0)\mathbf{X}_1 = \mathbf{F}_0, \tag{2.13}$$
$$\mathbf{A}_0(1)\mathbf{X}_1 + \mathbf{A}_1(1)\mathbf{X}_2 = \mathbf{F}_1. \tag{2.14}$$

Note that $\mathbf{A}_\alpha(n) = \mathbf{A}_\alpha, n \geqslant 2$ and also $\mathbf{X}_{-n} = -\mathbf{X}_n\ \forall n \geqslant 0$ and hence $\mathbf{X}_0 = \mathbf{0}$. Note also that because of symmetry the z-component of all displacements are zero and hence $\mathbf{X}_n \in \mathbb{R}^{20},\ |n| \geqslant 1$. For a defective Ti-centered domain wall with O1 or O3 atoms removed, $\mathbf{X}_0 \in \mathbb{R}^4$ (see Fig. 2.2).

The governing discrete boundary-value problem is closed by requiring boundedness of displacements at infinity, i.e.

$$\lim_{n\to\infty} \|\mathbf{X}_n\| < \infty. \tag{2.15}$$

One should note that the infinite crystal may undergo a rigid translation after relaxation. Condition (2.15) does not exclude this possibility. Note also that assuming that the domain wall is a mirror plane for displacements removes the translation invariance of the governing equations, i.e., those cores and shells that lie on the domain wall in the reference configuration remain on the domain wall after relaxation (i.e. $\mathbf{X}_0 = \mathbf{0}$).

When there are oxygen vacancies on the domain wall, one needs to look at boundary equations carefully. When modeling $PbTiO_3$ by a shell potential, an oxygen vacancy means removal of the core and shell of the oxygen atom and because we assume a charge-neutral oxygen vacancy, there will be a charge redistribution. This will affect the shell charges of the neighboring shells. It is known that charge redistribution is highly localized. Thus, in our calculations we distribute the charge $\Delta Q = Q_s + Q_c$, where Q_s and Q_c are oxygen shell and core charges, only to the fourteen first nearest neighbors of each oxygen vacancy. Most of the existing shell potentials have fixed charges. However, in a more realistic model shell charges should be variable to be able to adjust themselves to the environment, e.g., in the presence of a vacancy. There have been several efforts in the literature on building empirical charge-variable models for different systems based on Rappe and Goddard's charge equilibrium method [23] and its extensions. Here, we use a fixed-charge shell potential for $PbTiO_3$ and are not aware of any charge-variable shell model for this material. Therefore, we have to model the charge transfer due to oxygen vacancies approximately. However, this should not have severe effects on the results as our numerical tests show. We studied the sensitivity of solutions to the exact way of charge redistribution; we compared two cases: in the first case we distributed the charge equally to the nearest neighbors and in the second case we distributed the charge to nearest neighbors depending on their distances from the vacancy and assuming that charge distribution is exponentially decaying. We did not see much difference and thus in this work we distribute the charge equally between the nearest neighbors.

We consider three types of defective domain walls: (i) O2-defective, (ii) O1-defective, and (iii) O3-defective. An O2-defective domain wall is Pb-centered. See Fig. 2.1 for this notation. We see that the anharmonic lattice statics iterations do not converge in this case, i.e., this is not a stable configuration.[1] This is in agreement with ab initio calculations [11] that predict Ti-centered defective domain walls. O1 and O3-defective domain walls are Ti-centered with no O1 and O3 cores and shells, respectively, on the domain wall in the reference configuration (see Fig. 2.2).

The linearized governing equations can be solved exactly using the method proposed in [31]. Thus, we are able to solve the linearized governing equations exactly. Now to obtain the fully nonlinear solutions we use a modified Newton–Raphson iteration. Solving the linearized problem, we modify the reference configuration by imposing the harmonic displacements and then calculate the new unbalanced forces exactly using the interatomic potential [31]. Continuing in this manner, if there is an equilibrium configuration close to the chosen reference configuration, unbalanced forces converge to zero. In the present work, convergence means that all forces have magnitudes less than 0.05 eV/Å. Now, let us briefly explain the modified Newton–Raphson method, called the quasi-Newton method, that we use throughout this work.

Newton method is based on the following quadratic approximation near the current configuration $\mathscr{B}^k$:

$$\mathscr{E}(\mathscr{B}^k + \tilde{\boldsymbol{\delta}}^k) = \mathscr{E}(\mathscr{B}^k) + \nabla\mathscr{E}(\mathscr{B}^k)\cdot\tilde{\boldsymbol{\delta}}^k + \frac{1}{2}(\tilde{\boldsymbol{\delta}}^k)^{\mathsf{T}}\cdot\mathbf{H}(\mathscr{B}^k)\cdot\tilde{\boldsymbol{\delta}}^k + o\left(|\tilde{\boldsymbol{\delta}}^k|^2\right), \tag{2.16}$$

[1] This is also the case when the defective domain wall is under strain.

where $\tilde{\boldsymbol{\delta}}^k = \mathscr{B}^{k+1} - \mathscr{B}^k$ and $\mathbf{H}$ is the Hessian matrix. By differentiating the above formula with respect to $\tilde{\boldsymbol{\delta}}^k$, we obtain the Newton method for determining the next configuration $\mathscr{B}^{k+1} = \mathscr{B}^k + \tilde{\boldsymbol{\delta}}^k$:

$$\tilde{\delta}^k = -\mathbf{H}^{-1}(\mathscr{B}^k) \cdot \nabla \mathscr{E}(\mathscr{B}^k). \tag{2.17}$$

Note that in order to converge to a local minimum, the Hessian must be positive definite.

If the calculation of the Hessian in each iteration becomes numerically inefficient (like the present problem), one can use the quasi-Newton method. The main idea behind this method is to start from a positive-definite approximation to the inverse Hessian and to modify this approximation in each iteration using the gradient vector of that step. Close to the local minimum, the approximate inverse Hessian approaches the true inverse Hessian and we would have the quadratic convergence of the Newton method [22]. Here we use the Broyden–Fletcher–Goldfarb–Shanno (BFGS) algorithm [22] for generating the approximate inverse Hessian:

$$\mathbf{C}^{i+1} = \mathbf{C}^i + \frac{\tilde{\boldsymbol{\delta}}^k \otimes \tilde{\boldsymbol{\delta}}^k}{(\tilde{\boldsymbol{\delta}}^k)^{\mathsf{T}} \cdot \boldsymbol{\Delta}} - \frac{(\mathbf{C}^i \cdot \boldsymbol{\Delta}) \otimes (\mathbf{C}^i \cdot \boldsymbol{\Delta})}{\boldsymbol{\Delta}^{\mathsf{T}} \cdot \mathbf{C}^i \cdot \boldsymbol{\Delta}} + (\boldsymbol{\Delta}^{\mathsf{T}} \cdot \mathbf{C}^i \cdot \boldsymbol{\Delta})\mathbf{u} \otimes \mathbf{u}, \tag{2.18}$$

where $\mathbf{C}^i = (\mathbf{H}^i)^{-1}$, $\boldsymbol{\Delta} = \nabla \mathscr{E}^{i+1} - \nabla \mathscr{E}^i$, and

$$\mathbf{u} = \frac{\tilde{\boldsymbol{\delta}}^k}{(\tilde{\boldsymbol{\delta}}^k)^{\mathsf{T}} \cdot \boldsymbol{\Delta}} - \frac{\mathbf{C}^i \cdot \boldsymbol{\Delta}}{\boldsymbol{\Delta}^{\mathsf{T}} \cdot \mathbf{C}^i \cdot \boldsymbol{\Delta}}. \tag{2.19}$$

Calculating $\mathbf{C}^{i+1}$, one then should use $\mathbf{C}^{i+1}$ instead of $\mathbf{H}^{-1}$ to update the current configuration for the next configuration $\mathscr{B}^{k+1} = \mathscr{B}^k + \tilde{\boldsymbol{\delta}}^k$. If $\mathbf{C}^{i+1}$ is a poor approximation, then one may need to perform a linear search to refine $\mathscr{B}^{k+1}$ before starting the next iteration [22].

2.4. 180° Domain walls under strain

We put both the perfect and defective domain walls under normal and shear strains (see Fig. 2.1). We consider both compressive and tensile strains and also shear strains both along and opposite to the polarization directions. We apply strains to the defective lattice by imposing displacements in the proper directions far enough from the domain wall (displacements are in x- and y-directions for normal and shear strains, respectively). Note that the defective lattice is translated rigidly on both sides of the domain wall outside the computational box. Applying strain to the lattice should be done gradually. For both perfect and defective domain walls, we start with the strain-free relaxed domain wall configuration $\mathscr{B}$. Then, we apply proper boundary displacement to increase (or decrease) strain by the value $\Delta\epsilon$ to obtain the strained configuration $\mathscr{B}_{\Delta\epsilon}$. Note that $\Delta\epsilon$ should be small enough such that $\mathscr{B}$ and $\mathscr{B}_{\Delta\epsilon}$ are close to each other. In the present work, $\Delta\epsilon = 0.001$ for normal strains and $\Delta\epsilon = 0.0005$ for shear strains. Next, we start with $\mathscr{B}_{\Delta\epsilon}$ and calculate $\mathscr{B}_{2\Delta\epsilon}$. Repeating this procedure, one can apply large strains to the defective lattice and obtain its relaxed configuration $\mathscr{B}_\epsilon$ for a given strain ϵ. Using the notation of the previous sections, we summarize our algorithm for applying strain as follows.

Input data: $\mathscr{B}_\epsilon, \Delta\epsilon$ (strain increment)
- Initialization
  - Apply B.C. to $\mathscr{B}_\epsilon$ and obtain $\mathscr{B}^1$
  - $\mathbf{H}^1 = \mathbf{H}|_{\mathscr{B}=\mathscr{B}^1}$ and set $\mathbf{C}^1 = (\mathbf{H}^1)^{-1}$
- Do until convergence is achieved
  - Calculate forces
  - Use quasi-Newton method to calculate $\mathbf{C}^{k+1}$
  - Use $\mathbf{C}^{k+1}$ to obtain $\mathscr{B}^{k+1}$
- End Do
- End

3. Numerical results

3.1. Perfect domain walls

In our numerical examples we show the anharmonic displacements with respect to the reference configuration. The first step is to calculate unbalanced forces. Our choice of reference configurations makes the unbalanced forces localized in the direction perpendicular to the domain wall. However, one should note that a domain wall is an extended defect and unbalanced forces are not localized in the tetragonal c-direction. We are able to handle this nonlocality issue using the symmetry reduction idea. Since core and shell displacements are close, we only report the core displacements in this section. We assume $2N$ unit cells in the simulation box (see Fig. 2.1). Our numerical experiments show that $N = 10$ would be enough for calculating displacements as the structure does not changed by using larger values for N.

Fig. 3.1 shows the displacements of Pb and Ti cores in the a- and c-directions (u_a and u_c, respectively) for a perfect Ti-centered domain wall under axial strain ϵ_x. We plot the displacements for different values of the axial strain between -0.03 and 0.03. As expected, u_a has a larger variation than u_c under the axial strain. However, note that axial strain does not have a significant effect on domain wall thickness; it is seen that all the distortions occur within two lattice spacings on each side of the domain wall, i,e. domain wall thickness is about 1.0–1.5 nm regardless of the value of the axial strain. Fig. 3.2 shows displacements of the same domain wall under different values of shear strain γ_{xy}. The c-displacements are in the polarization direction for negative values of γ_{xy} and are in the opposite direction for positive values of γ_{xy}. Hence, we do not see symmetric displacements with respect to the unstrained structure. Also, we observe that unlike axial strains, shear strains have a considerable effect on both u_a and u_c. Similar results for a perfect Pb-centered domain wall are shown in Figs. 3.3 and 3.4.

3.2. Domain walls with oxygen vacancies

We report the displacements of a Ti-centered 180° domain wall with oxygen vacancies under axial and shear strains. Since displacements of O1-defective and O3-defective walls are similar, here we only report the results for O1-defective walls. Fig. 3.5 shows the displacements for an O1-defective domain wall under normal strain. O1 vacancies lie on the domain wall and because of symmetry have zero displacements, i.e. they will stay on the domain wall after deformation. For the strain-free configuration, all distortions parallel to the domain wall (c-displacements) occur within two lattice spacings on each side of the wall, i.e., thickness of the domain wall in c-direction is not affected by oxygen vacancies. However, it is seen that structure is significantly different from that of a perfect domain wall. It is also seen that unlike perfect domain walls, a-displacements have the same order of magnitude as the corresponding c-displacements. We observe that the a-displacements are nonzero within three lattice spacings on each side of the wall. Thus, the thickness of an O1-defective domain wall is about 1.5–2.0 nm, i.e. oxygen vacancies increase the domain wall thickness by about 50%. Here similar to perfect domain walls, we see that normal strains do not have a significant effect on the thickness of the domain wall. Fig. 3.6 shows the displacements of an O1-defective domain wall under shear strain. Again, we see that shear strain has a significant effect on the displacements of the domain wall. Also note that domain wall thickness increases in a-direction, but this increase is less than the increase observed for perfect wall (see Fig. 3.2).

The only restriction in our calculations is the high density of oxygen vacancies (similar to the existing ab initio calculations). The resulting stiffness coefficient matrices become highly

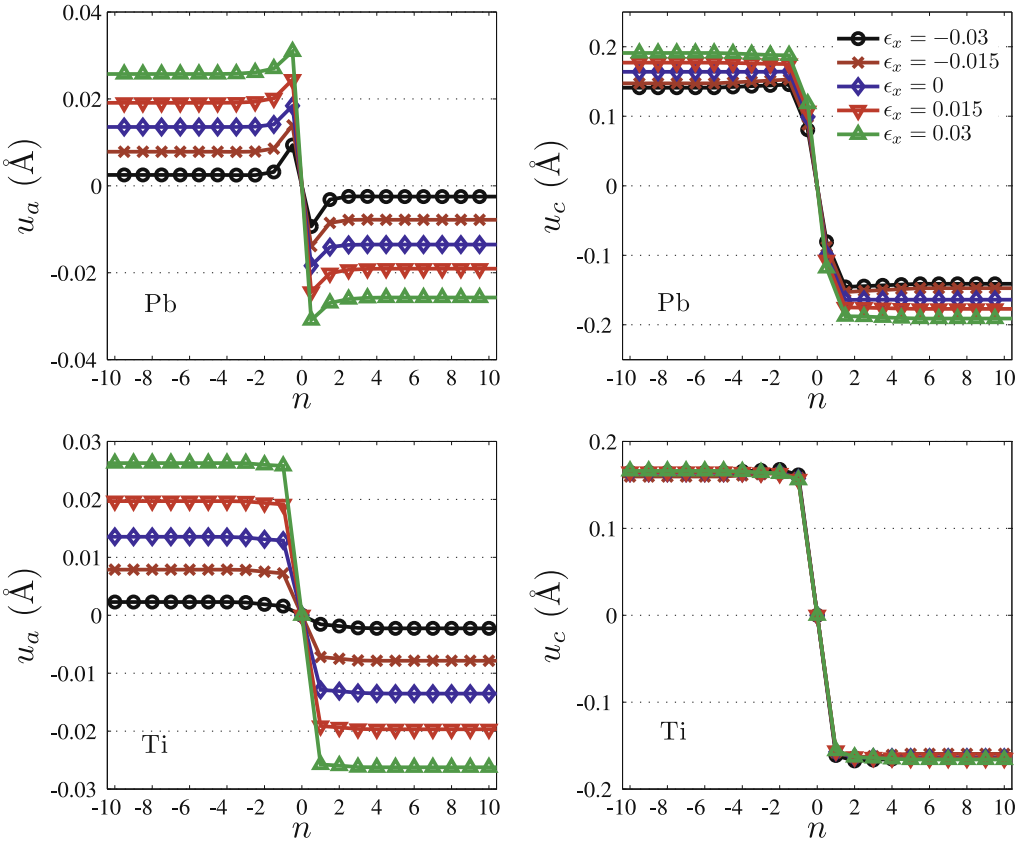

Fig. 3.1. a- and c-structure of a perfect Ti-centered 180° domain wall under axial strain ϵ_x. u_a and u_c are displacements along a-direction and the tetragonal c-direction, respectively.

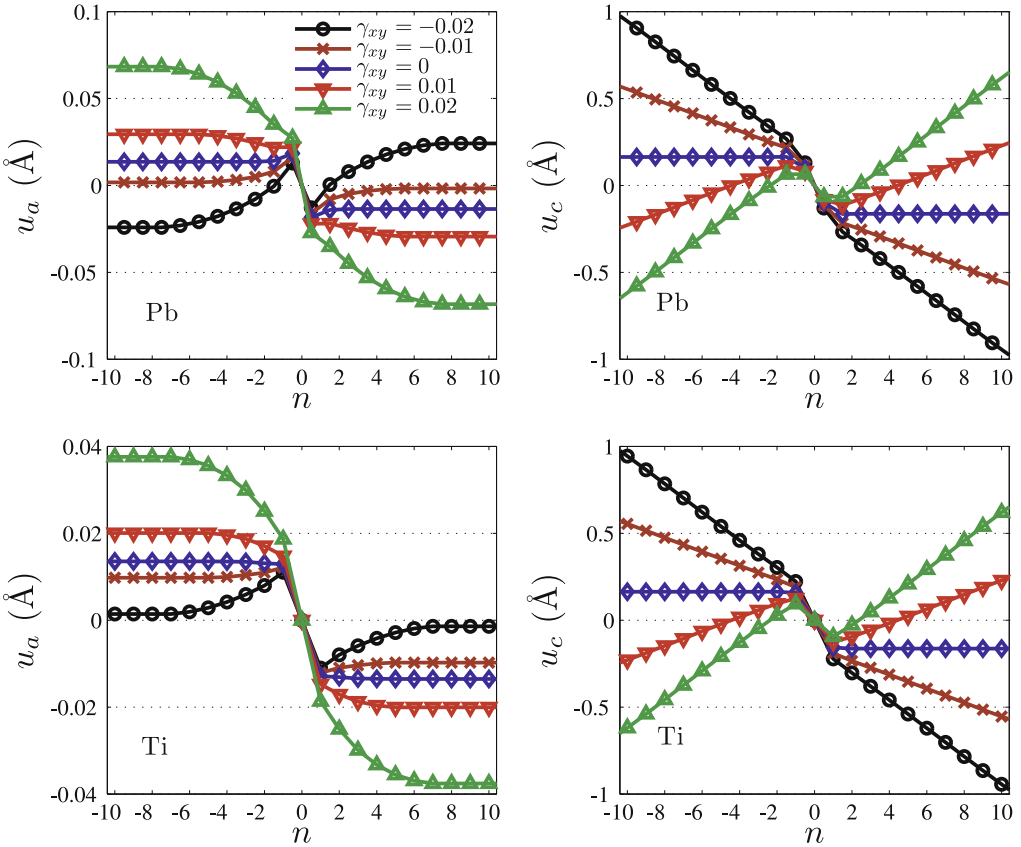

Fig. 3.2. a- and c-structure of a perfect Ti-centered 180° domain wall under shear strain γ_{xy}. u_a and u_c are displacements along a-direction and the tetragonal c-direction, respectively.

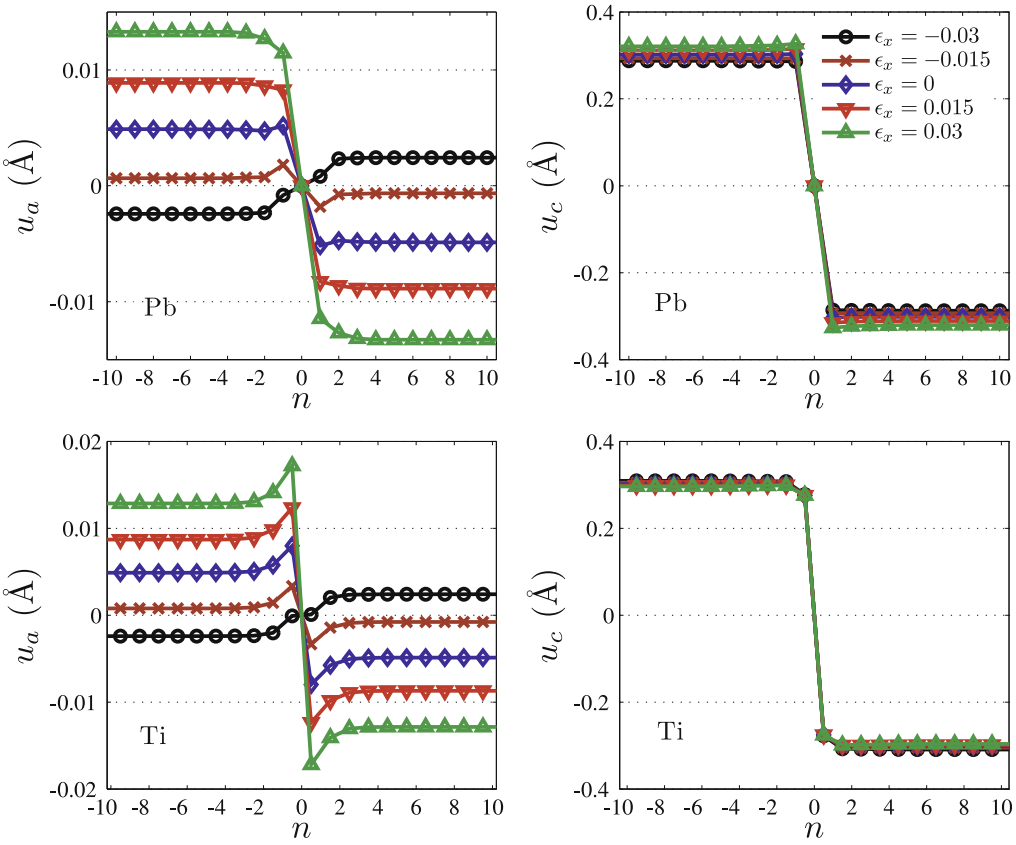

Fig. 3.3. a- and c-structure of a perfect Pb-centered 180° domain wall under axial strain ϵ_x. u_a and u_c are displacements along a-direction and the tetragonal c-direction, respectively.

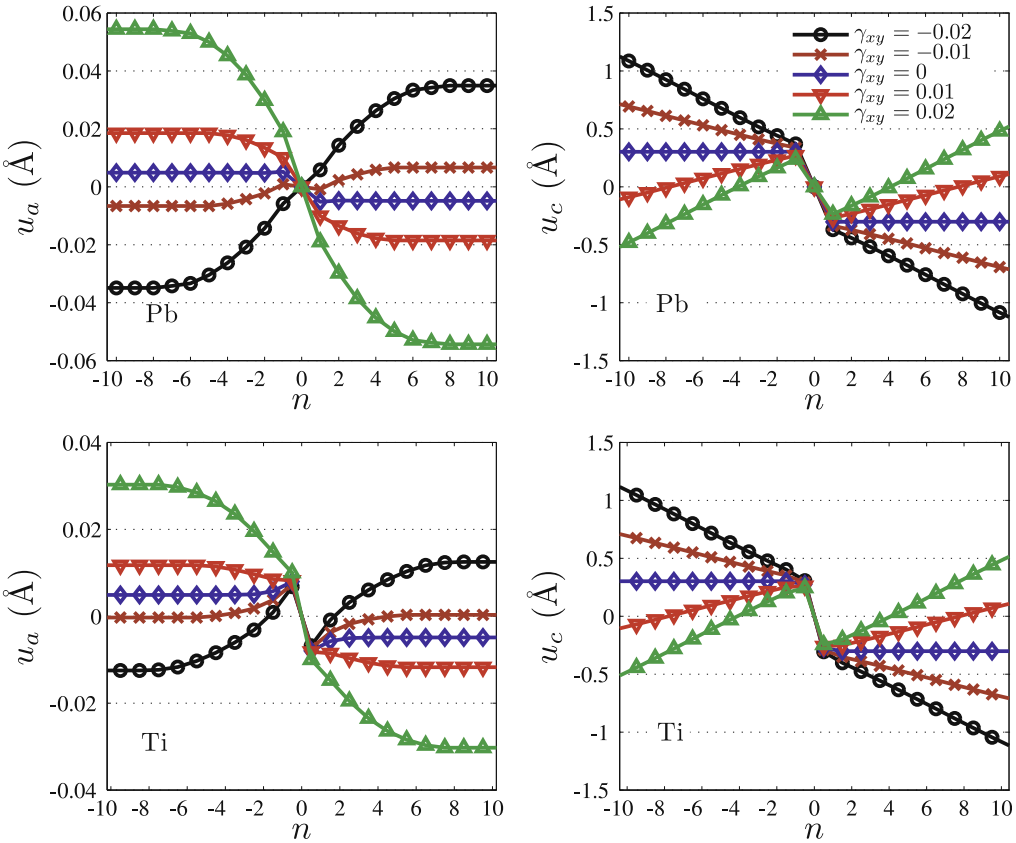

Fig. 3.4. a- and c-structure of a perfect Pb-centered 180° domain wall under shear strain γ_{xy}. u_a and u_c are displacements along a-direction and the tetragonal c-direction, respectively.

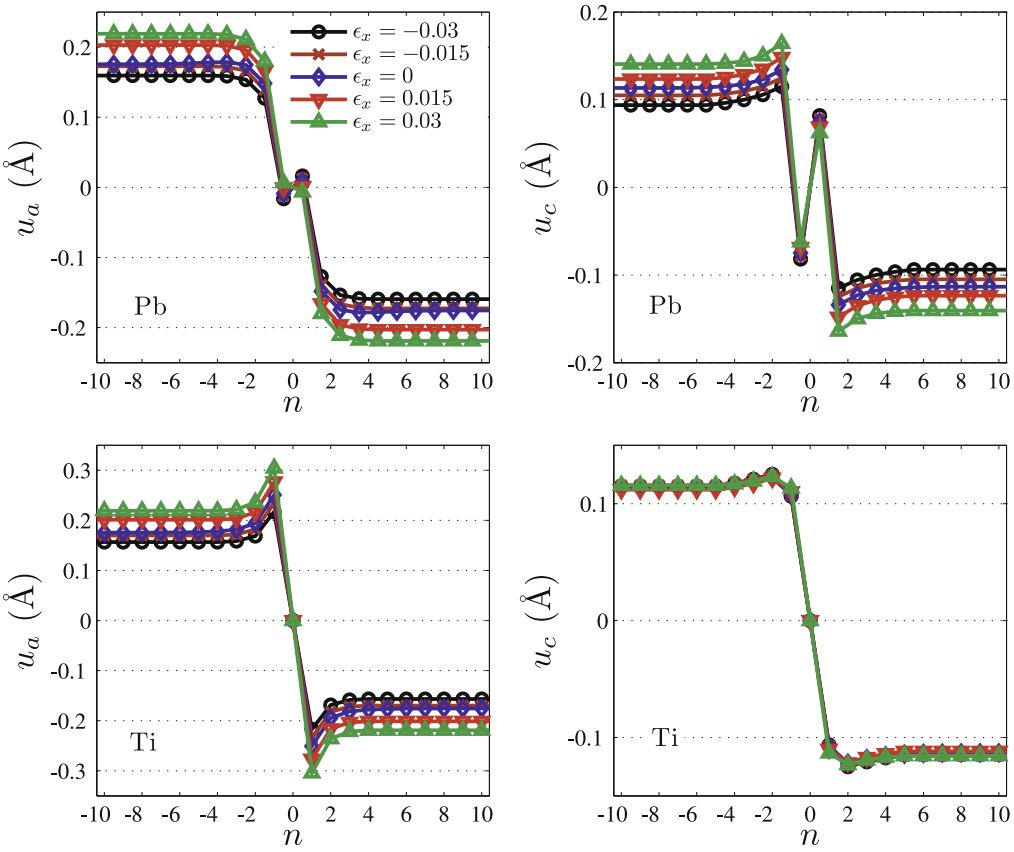

Fig. 3.5. a- and c-structure of an O1-defective 180° domain wall under axial strain ϵ_x. u_a and u_c are displacements along a-direction and the tetragonal c-direction, respectively.

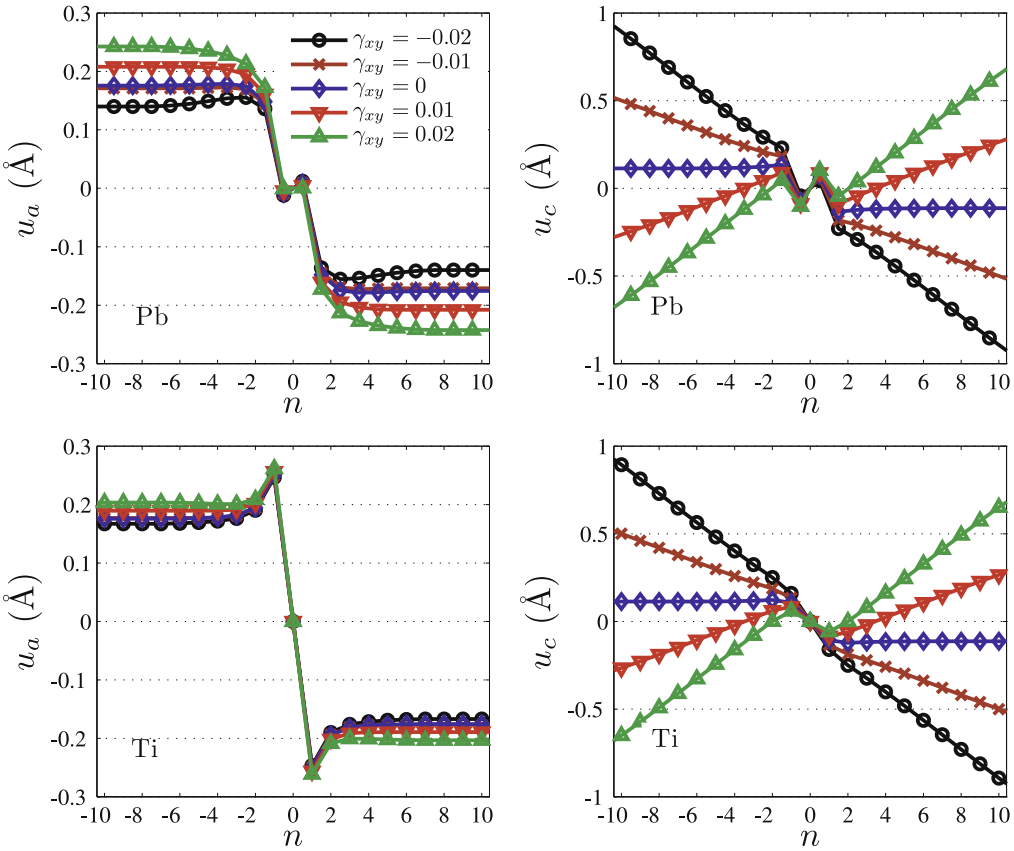

Fig. 3.6. a- and c-structure of an O1-defective 180° domain wall under shear strain γ_{xy}. u_a and u_c are displacements along a-direction and the tetragonal c-direction, respectively.

ill-conditioned by increasing the period of vacancies. Therefore, we did the calculations only for the three cases where all O1, O2, or O3 oxygen atoms are removed from the domain wall. In all the three cases unbalanced forces in the tetragonal *c*-direction are nonzero only in two unit cells on each side of the wall. We checked this for several lower density arrangements of oxygen vacancies and observed the same local property for unbalanced forces. In the case of perfect domain walls, unbalanced forces perpendicular to the wall are very small and nonzero only in two layers on each side of the wall. In the case of defective domain walls, these unbalanced forces are nonzero in three unit cells on each side of the wall. This was also the case for several other lower density arrangements of oxygen vacancies on the wall. Thus, we believe that the high density of oxygen vacancies does not have a significant effect on the thickness of the defective domain wall, although it affects the structure. In other words, lowering the density of oxygen vacancies we expect to see changes in structure but no significant change in thickness.

4. Concluding remarks

In this paper, we presented a semi-analytic study of the effect of oxygen vacancies and strain on the structure of 180° domain walls in $PbTiO_3$ using a shell potential. We considered both Pb-centered and Ti-centered domain walls with oxygen vacancies sitting on them. We observed that Pb-centered domain walls with oxygen vacancies are not stable (even under strain) and this is in agreement with the recent ab initio calculations that predict Ti-centered defective domain walls. To be able to solve for the structure of defective domain walls semi-analytically we have to work with a high density of oxygen vacancies on the domain wall (similar to the existing ab initio calculations). However, we believe that density of oxygen vacancies does not have a noticeable effect on the thickness of the defective domain wall.

We observe that oxygen vacancies change the structure of a 180° domain wall significantly. One important effect of oxygen vacancies is that in the presence of oxygen vacancies, displacements perpendicular to the domain wall are of the same order of magnitude as the displacements in the tetragonal *c*-direction. In the anharmonic lattice statics iterations we observe that *a*-displacements have a fairly long tail, about five lattice spacings on each side of the wall. However, the thickness of a defective 180° domain wall is about 1.5 times that of a perfect domain wall. This is different from the results of a recent experimental study of 90° domain walls in $PbTiO_3$ using AFM and the observed large variations of domain wall thickness in the internal 0.5–4.0 nm [28]. However, our results are in agreement with those obtained from a recent continuum model that predicts different behaviors of 180° and 90° in response to point defects [30]. We studied the effect of strain on both perfect and defective 180° domain walls. We observed that normal strains have a greater effect on *a*-displacements but shear strains have a significant effect on both *a*- and *c*-displacements. Finally, we observe that the domain wall thickness does not change significantly under normal or shear strains.

Acknowledgment

We benefitted from a discussion with V. Gavini.

References

[1] A. Asthagiri, Z. Wu, N. Choudhury, R.E. Cohen, Ferroelectrics 333 (2006) 69.
[2] K. Bhattacharya, G. Ravichandran, Acta Materialia 51 (2003) 5941.
[3] M. Born, K. Huang, Dynamical Theory of Crystal Lattices, Oxford, 1988.
[4] R. Bujakiewicz-Koronska, Y. Natanzon, Integrated Ferroelectrics 108 (2009) 21.
[5] M. Calleja, M.T. Dove, E.K.H. Salje, Journal of Physics: Condensed Matter 15 (2003) 2301.
[6] E. Cockayne, B.P. Burton, Physical Review B 69 (2004) 144116.
[7] B.G. Dick, A.W. Overhauser, Physical Review 112 (1964) 90.
[8] M. Dawber, K.M. Rabe, J.F. Scott, Review of Modern Physics 77 (2005) 1083.
[9] C. Franck, G. Ravichandran, K. Bhattacharya, Applied Physics Letters 88 (2006) 102907.
[10] V. Gopalan, V. Dierolf, D.A. Scrymgeour, Annual Review of Materials Research 37 (2007) 449.
[11] L.X. He, D. Vanderbilt, Physical Review B 68 (2001) 134103.
[12] H. Kanazaki, Journal of Physics and Chemistry of Solids 2 (1957) 24.
[13] S. Kavianpour, A. Yavari, Computational Materials Science 44 (2009) 1296.
[14] W.T. Lee, E.K.H. Salje, U. Bismayer, Physical Review B 72 (2005) 104116.
[15] T.J. Matsubara, Journal of Physical Society of Japan 7 (1952) 270.
[16] B. Meyer, D. Vanderbilt, Physical Review B 65 (2001) 1.
[17] M. Ortiz, R. Phillips, Advances in Applied Mechanics 59 (1999) 1217.
[18] J. Padilla, W. Zhong, D. Vanderbilt, Physical Review B 53 (1996) R5969.
[19] C.H. Park, D.J. Chadi, Physical Review B 57 (1998) R13961.
[20] S. Pöykkö, D.J. Chadi, Applied Physics Letters 75 (1999) 2830.
[21] S. Pöykkö, D.J. Chadi, Journal of Physics and Chemistry of Solids 61 (2000) 291.
[22] W.H. Press, S.A. Teukolsky, W.T. Vetterling, B.P. Flannery, Numerical Recipes: The Art of Scientific Computing, Cambridge University Press, 1989.
[23] A.K. Rappe, W.A. Goddard III, Journal of Physical Chemistry 95 (1991) 3358.
[24] J.F. Scott, M. Dawber, Applied Physics Letters 76 (2000) 3801.
[25] M. Sepliarsky, R.E. Cohen, 2000, Development of a shell model potential for molecular dynamics for $PbTiO_3$ by fitting first principles results, in: R.E. Cohen (Ed.), Fundamental Physics of Ferroelectrics, pp. 36-44.
[26] M. Sepliarsky, Z. Wu, A. Asthagiri, R.E. Cohen, Ferroelectrics 301 (2004) 55.
[27] J.K. Shang, X. Tan, Acta Materialia 49 (2001) 2993.
[28] D. Shilo, G. Ravichandran, K. Bhattacharya, Nature Materials 3 (2004) 453.
[29] T. Shimada, Y. Umeno, T. Kitamura, Physical Review B 77 (094105) (2008) 1.
[30] Y. Xiao, V.B. Shenoy, K. Bhattacharya, Physical Review Letters 95 (2005) 247603.
[31] A. Yavari, M. Ortiz, K. Bhattacharya, Philosophical Magazine 87 (26) (2007) 3997.
[32] A. Yavari, M. Ortiz, K. Bhattacharya, Journal of Elasticity 86 (2007) 41.
[33] Q. Zhang, 2004. Atomistic Simulations of Barium Titanate, Ph.D. Thesis, California Institute of Technology.